Timing of the southward retreat of the ITCZ at the end of the Holocene Humid Period in Southern Arabia: Data-model comparison

Anne-Marie Lézine, Sarah J. Ivory, Pascale Braconnot, Olivier Marti

Timing of the southward retreat of the ITCZ at the end of the Holocene Humid Period in Southern Arabia: data-model comparison

Anne-Marie Lézine[1], Sarah J. Ivory[2], Pascale Braconnot[3], Olivier Marti[3]

[1] Sorbonne Universités, UPMC, Univ Paris 06, CNRS-IRD-MNHN, LOCEAN/IPSL laboratory, 4 place Jussieu, 75005 Paris, France

[2] Department of Earth, Environmental, and Planetary Sciences, Brown University, Providence, RI 02912

[3] Laboratoire des Sciences du Climat et de l'Environnement/IPSL, CEA-CNRS-UVSQ – UMR8212, CE Saclay, l'Orme des Merisiers, 91191 Gif-sur-Yvette Cedex, France

Corresponding author: anne-marie.lezine@locean-ipsl.upmc.fr

Abstract

New pollen data from Omani mangroves (Kwar-al-Jaramah [22.49° N - 59.76° E] and Filim [20.61° N - 58.17° E]), in addition to previously published paleohydrological records from Southern Arabia improve our understanding of the timing and amplitude of the southward retreat of the Indian monsoon influence in Southern Arabia along a north-south transect. Comparison with simulations performed with the IPSL climate model, considering both snapshot experiments and transient simulations from 6000 cal yr BP to the present, confirm the latitudinally time-transgressive nature of the humid-arid transition at the end of the Holocene Humid Period. This occurred in two steps, respectively dated at around 5000 and 2700 cal yr BP. At around 5000 cal yr BP, the southward ITCZ shift was orbitally-driven and led to the abrupt aridification at Kwar-al-Jaramah and the progressive increase of dryness at

Filim as the mean position of the ITCZ was centered ca 22.30°N. At 2700 cal yr BP, aridity was fully in place over all of southern Arabia due to increased climate variability. More intense rainy events during the last millennium, however, may have contributed to the discrete hydrological improvement without any impact on the regional vegetation which has remained desert to the present day.

Key words: Pollen, climate simulations, IPSL model, Oman, ITCZ, end of the Holocene Humid Period

1. Introduction

The timing and amplitude of the end of the Holocene Humid Period and the transition toward the present day arid/semi-arid conditions in the northern tropics has been the subject of multiple debates involving numerous scientists from both the model (e.g., Claussen and Gayler, 1997; Claussen et al., 2003; Liu et al., 2007) and data communities (e.g., deMenocal et al., 2000; Kröpelin et al., 2008a and b, Bayon et al., 2012). Several scenarios have been developed to discuss the abrupt or gradual character of this period and to identify the forcings at work (e.g., Brovkin et al., 2002; Rensen et al., 2006). These debates have mostly focused on regions under the Atlantic monsoon influence, with a specific emphasis on the iconic "Green Sahara". This region is well known to have hosted flourishing prehistoric cultures evidenced by widespread archaeological remains (e.g., Kuper and Kröpelin, 2006; Manning and Timpson, 2014), rock paintings and carvings (Le Quellec, 2013), and abundant tropical faunas (e.g., Jousse and Escarguel, 2006) during the Holocene. Based on paleohydrological (Lézine et al., 2011) and archaeological (Kuper and Kröpelin, 2006) evidence, it has been shown that the end of the "Green Sahara" period in northern tropical

Africa and the start of present day arid conditions has been latitudinally time-transgressive, with the lake phase ending from 6500 cal yr BP between 26° and 28°N to 3500 cal yr BP between 16° and20° N. In this region, however, the response time of the systems (hydrology, vegetation), involving aquifer recharge or surficial runoff from distant origin and/or from the Saharan highlands make the evaluation of the precise timing of the climate signal alone difficult (Gasse, 2000; Lézine et al., 2011; Hély and Lézine, 2014).

The end of the Holocene Humid Period is also recorded in regions under the Asian summer monsoon influence by a dramatic weakening of rainfall ca 5000-4000 cal yr BP (e.g., Morrill et al., 2003), particularly in its western part (e.g., Ivory et al., 2009; Lézine et al., 2014). Here also dramatic impact of changing climate on past Harappan culture in the Indus Valley has been evoked (Farooki et al., 2013). In this paper, we focus our attention on southern Arabia, a region particularly suitable for investigating the late Holocene period owing to the quality of the available high-resolution records. Paleolakes are particularly scarce and poorly preserved due to the exceptionally arid conditions which prevail in the Rub-al-Khali desert today (e.g., Lézine et al., 2007; 2014). However, speleothems records in South-Eastern Arabia have led to observation of changing rainfall amounts at the study sites as well as changes in the origin of the rains (Neff et al. 2001, Fleitmann et al., 2003; 2007). In addition, specific geomorphological and ecological features in coastal areas favor the preservation of mangroves whose floristic composition is closely dependent on rainfall amount and distribution (Spalding et al., 1997). These sedimentary environments also have the advantage of rapid depositional rates and good preservation of the organic matter, and thus are powerful tools to trace fluctuations of the rain belt associated with past monsoon circulation and changes in the location of the Intertropical Convergence Zone (ITCZ) through time (Lézine et al., 2002; Berger et al., 2013).

We consider here new pollen data from Omani mangroves and compare the chronology of events with those deduced from the isotopic composition of speleothems and the extension of lakes and wetlands. Our aim is to discuss the timing and amplitude of the southward retreat of the Indian monsoon influence in Southern Arabia along a north-south transect from 23° to 17°N. The results of these new data are compared with results of simulations with the IPSL climate model (Dufresne et al., 2013), considering both snapshot experiments for key Holocene periods and a suite of transient simulations. This allows us to discuss the changes induced by long term alterations to Earth's orbit and provide an indication of the possible role of insolation in triggering some of the rapid changes observed in the pollen records. The remainder of the manuscript is organized as follows: section 2 presents the new records and the climate simulations, whereas section 3 discusses the timing of the environmental changes over the region of interest and their relationship to the southward shift of the ITCZ from the mid-Holocene to today. A conclusion is provided in section 4.

2. Mid to late Holocene pollen records and climate simulations

2.1 Regional climate features

Oman is situated at the present northern limit of the annual migration of the ITCZ and the associated rainfall belt. In summer, southwesterly surface winds carry moisture from the southern Indian Ocean along the Arabian coast but do not penetrate far north- and eastwards into Southern Arabia (Fig. 1). The mean annual rainfall rapidly decreases from the southernmost part of the peninsula (the mountains of Yemen) to the Dhofar region in South Oman to the east, where the coastal station of Salalah records about 83 mm of annual rainfall. SW monsoon fluxes barely penetrate the Gulf of Oman, and rains only rarely occur in the lowlands where dry conditions occur year round. In winter, the southward penetration

of Mediterranean cyclonic depressions follows the topographic corridor of the Arabo-Persian Gulf bounded by the Zagros Mountains, Iran, to the north-east and the Jebel-al-Akhdar range, Oman, to the southwest. Winter rainfall averages 90 mm along the coast and reaches up to 350 mm in the Jebel-al-Akhdar, where snow may also occur. Mean annual temperature varies from about 26°C at Salalah to 35°C at Muscat along the Gulf of Oman, with temperature falling with altitude from about 0.6°C per 100 m elevation in the Jebel-al-Akhdar (Gazanfar and Fischer, 1998).

2.2 Sediment cores

Two cores were collected at Kwar-al-Jaramah (KAJ) in the Gulf of Oman (22.49°N - 59.76°E) and at Filim at the Indian Ocean shore (20.61°N - 58.17°E) (Figs. 1 and 2). Both were recovered behind the forest remnants of *Avicennia marina*-dominated mangrove populations. Kwar-al-Jaramah (Lézine, 2009) is a sheltered creek fed by local wadis originating from the foothills of the Jebel al Akhdar (El-Baz, 2002). Filim is a bay located west of the Barr al Hikmân peninsula facing the Masirah island. It is fed by the wadi Halfayn/wadi Andam system originating from the Jebel al Akhdar, located several hundreds of kilometers to the north. The regional environment is of desert type at both sites, and the mangrove is only represented by a single species, *Avicennia marina,* which is particularly adapted to highly saline environments (Spalding et al., 1997).

The sedimentary columns are 440 cm long at both sites and consist of homogenous sandy mud with rare shell fragments. Chronologies are based on seven AMS ^{14}C ages on carbonates at Kwar-al-Jaramah and eight at Filim. Raw radiocarbon dates were reservoir-corrected (Saliège et al., 2005) and converted to calibrated ages using CALIB Radiocarbon Calibration software (Reimer et al., 2009). Then, a time scale was obtained by linear interpolation

between two ages taking into account the highly variable sedimentation rate in such a littoral environments undergoing sea level fluctuations (Lambeck, 1996) (Table 1a and b).

2.3 Pollen analysis

Ninety seven samples (each 1.5–3 cm^3) were taken for pollen analyses. Samples were processed according to standard procedures (chemical treatment with HCL and HF; sieving at 5 µm) (Faegri and Iversen, 1975). They yielded an abundant microflora of 163 pollen taxa for pollen counts ranging between 299 to 463 at KAJ and 82 to 405 at Filim. Pollen grains were determined using pollen flora of Qatar (El-Ghazaly, 1991), Chad (Maley, 1970), and East Africa (Bonnefille and Riollet, 1980). Littoral mangrove pollen percentages (*Rhizophora* and *Avicennia*) were calculated against the sum of all the pollen grains and fern spores counted. As usual in tropical marine and littoral palynology, these taxa were excluded from the pollen sum for the calculation of the percentages of the other pollen taxa originating from inland vegetation types in order to better represent the regional flora (Fig. 3).

Pollen analysis reveals that the southernmost site, Filim, is remarkably diverse, with 133 taxa including 46 trees and shrubs (AP), compared to Kwar-al-Jaramah, where only 103 taxa were identified, including 29 AP (Supplementary Table 1). This is mainly due to the proximity of the Dhofar region, an area of tropical phytogeographical affinity restricted to the escarpments of SW Oman/SE Yemen (Miller and Morris, 1988). The Dhofar escarpment is a crescent-shaped arc directly influenced by the Indian summer monsoon rains. In addition, cold sea surface temperatures from nearby upwelling maintains mists and clouds on its slopes allowing tropical plants to grow. The occurrence, even in small percentages, of numerous tropical taxa at Filim (e.g., *Rhus, Pistacia, Maerua, Boscia/Cadaba, Albizia,*

144 *Andrachne*) testifies to regional pollen transport by SW-NE (summer monsoon) wind fluxes
145 and also, probably, the eastward expansion of this particular region during the Holocene.
146 Four main features emerge from the pollen assemblages allowing characterization of two
147 main pollen zones at Filim and three at Kawr-al-Jaramah (KAJ – Lézine, 2009) (Fig. 3):
148 (1) the dominance of desert/halophytic herbaceous plant communities (mainly
149 Amaranthaceae/Chenopodiaceae, Asteraceae, *Artemisia*, Poaceae, and Cyperaceae) from
150 about 7000 cal yr BP to the present;
151 (2) a dramatic change in mangrove composition. Two mangrove taxa are present: *Avicennia*
152 *marina* and *Rhizophora mucronata*. *Rhizophora mucronata* is typically a tropical species
153 which requires freshwater from both rivers and summer rainfall (Spalding et al., 1997). It is
154 absent today from the Omani mangroves. However, paleoenvironmental studies testify to its
155 occurrence in the Northern Indian Ocean sector during the Holocene (Overpeck et al., 1996)
156 and, particularly along the coasts of Southern Arabia at Suwayh (22°05N) (Lézine et al., 2002)
157 or even northward (Tengberg, 2005). In Arabia, relict communities of *Rhizophora* persist
158 today in only two restricted sectors: the Kamaran island in the Red Sea and near al-
159 Hudaydah at 15.24°N. *Avicennia marina* is a mangrove species which has a high tolerance of
160 salinity. It is widely distributed in the dry, desert coastal zones of Arabia, and it reaches up to
161 27°N in the Arabo-Persian Gulf and 28°N in the Red Sea;
162 (3) the growing importance toward the end of the period studied of *Prosopis cineraria*.
163 *Prosopis cineraria* is a native species of Saharo-Sindian vegetation zone, a region influenced
164 by a bi-seasonal, Mediterranean-type climate with a rain maximum during winter and spring
165 (Ghazanfar and Fisher, 1998). In Oman, its distribution encompasses the coastal plains along
166 the Arabo-Persian Gulf, where rainfall is too low to maintain a typical tropical vegetation.

Modern pollen samples from this region do not record percentages of *Prosopis cineraria* higher than 9% (1.6% in average) (Lézine et al., 2000).

(4) pollen transport from distant origin, mainly afro-montane (e.g., Ericaceae*, Juniperus, Myrica, Olea europea, Podocarpus)* which is recorded at both sites. These taxa can originate either from Jebel-al-Akhdar to the north-east or from the Dhofar escarpment to the south-west in Oman, but also from more remote regions such as the highlands of Yemen or the Horn of Africa.

The pollen zones are as follows:

Filim zone 1 (6800-2700 cal yr BP) is characterized by the presence of *Rhizophora,* the percentages of which reach up to 52%. Pollen grains from tropical plant communities are present, in scattered occurrence and low values. *Rhizophora* percentages decrease toward the end of this zone in two steps successively dated from 6800 to 5100 cal yr BP (52 to 20%) and from 5100 to 2700 cal yr BP (20% to 0). *Artemisia,* from desert/halophytic herbaceous plant communities, displays an opposite trend with values regularly increasing from 2% to 23%.

Filim zone 2 (2700 cal yr BP - present) is characterized by the disappearance of *Rhizophora,* which is replaced by *Avicennia,* the percentages of which increase from 0 to 4% toward the end of this zone. This zone is also characterized by the appearance, even in low percentages, of *Prosopis cineraria*. This taxon is associated with other semi-desert elements (*Salvadora, Maerua, Moltkiopsis*)

KAJ zone 1 (6300- 4500 cal yr BP) is characterized by the presence of *Rhizophora,* which reaches a maximum of 13%. It is also associated with *Avicennia* abundances of 3 - 7%.

KAJ zone 2 (4500-2700 cal yr BP). *Rhizophora* almost disappears from this zone whereas, *Avicennia* remain constant. *Artemisia* percentages slightly increase compared to the preceding zone (max = 11%).

KAJ zone 3 (2700 cal yr BP – present) records the progressive increase of *Prosopis cineraria,* which reaches up to 11% in the uppermost levels, and the significant decrease of the mangrove pollen types: *Rhizophora* is rare with values less than 0.2%. *Avicennia* decreases to percentages of 0.9%

2.4 Climate simulations with the IPSL-CM5 model

Simulations of the mid to late Holocene were run with the same IPSL model version as the one used for the last CMIP5 ensemble of simulations (Dufresne et al., 2013). IPSL_CM5A is a state-of-the-art coupled global general circulation model. It couples the LMDz atmosphere model (Hourdin et al., 2006), with a horizontal resolution of 96 × 96 grid points and a vertical resolution of 39 levels, to the ocean model NEMO/OPA with 182 grid points in longitude × 149 in latitude and 31 vertical levels (Madec et al., 1997), using the coupler OASIS (Valcke, 2006). The land surface model ORCHIDEE is coupled to the atmosphere model and includes a river runoff scheme to close the water budget between land and ocean (Krinner et al., 2005). The sea-ice model LIM2 (Fichefet and Maqueda, 1997) is coupled to both atmosphere and ocean models. The carbon cycle is interactive in the ocean and in the land-surface. For the latter, the leaf area index is also fully interactive but vegetation is prescribed. Vegetation feedback is therefore partly represented in these simulations (Kageyama et al., 2013; Braconnot and Kageyama, 2015).

We consider both time slice experiments for the mid-Holocene (6 ka), the late Holocene (4 ka), and the preindustrial period (PI, 0 ka), in addition to transient late Holocene

213 experiments starting from the 6 ka simulation. The model and mid-Holocene simulations are
214 presented in Kageyama et al. (2013), and the 4 ka simulation is discussed in Saint-Lu et al.
215 (2015). These time slice simulations consider only the changes in Earth's orbital parameters
216 which are prescribed following Berger (1978) as shown in table 2. The mid-Holocene
217 simulation considers in addition the small changes in greenhouse gases, following the PMIP3
218 protocol (Braconnot et al., 2012). Each time slice simulation is 1000 years long, and the
219 annual mean cycles and wind rose statistics where computed from the last 500 years of each
220 simulation.
221 The model underestimates the northward extent of monsoon rain over the Sahel today
222 (Kageyama et al., 2013). Despite the precipitation bias over land, the simulated changes at 6
223 ka resemble the one produced by the ensemble PMIP3 simulation (Braconnot et al., 2012;
224 Harrison et al., 2015). The major characteristics of the difference in African and Indian
225 monsoon are consistent with the results obtained by Marzin and Braconnot (2009) with the
226 previous version of the IPSL model. This is also the case for the 4 ka simulation over the
227 southern hemisphere convergence zone (Saint-Lu et al., 2015). Interestingly, the monsoon
228 flow is well represented over the Arabian Sea and along the coast as depicted by boreal
229 summer surface winds in Figure 4. Monsoon precipitation is underestimated in Africa and
230 India, but slightly overestimated in the northeastern part of the Arabian Sea. Figure 4 shows
231 the reduction of the SW monsoon flow in July-August from the mid-Holocene to present day,
232 together with the increase of the NE boreal winter monsoon flow. Monthly wind direction
233 anomalies highlight the higher frequency of S-SW winds at 6 ka and strengthening of the
234 wind from in the western quadrant from W-NW to S. During boreal winter the changes in
235 frequency and intensity reflect a slight wind rotation from the N-NE to the NE.

The initial state of the PMIP3 transient simulations is from IPSL of the mid-Holocene climate (6 ka) described in Kageyama et al. (2013). We performed two simulations with an acceleration in the orbital parameters by a factor 10, following Lorenz and Lohmann (2004) (Fig. 5). With this acceleration, a 600 year-long simulation represents 6000 climate years. The orbital parameters (Table 2) vary with time and, because of the acceleration, the 4ka values are found for year 200 and those of PI for year 600. The long term trend can be attributed to the long term insolation forcing, but the short term variability represents only inter-annual to centennial variability, and not millennium scale variability. These two simulations start from different initial dates in the 6 ka simulation. The third simulation is a fully synchronous experiment in which the orbital parameters are updated every year. This experiment only covers the 2500 years from 6000 to 3500 cal yr BP. Due to storage problems, a period of time is missing in the model outputs between 4800 and 4750 cal yr BP. The representation of the monsoon has the same quality and biases as the ones highlighted above for the time slice experiments.

Figure 5 shows the evolution of precipitation as a function of time, comparing the accelerated and non-accelerated simulations for three latitudinal bands over the region 20°N-24°N, 18°N-20°N and 14°N-18°N. As expected, precipitation is characterized in the three latitudinal bands by a long term decreasing trend over this period that can be related to the long term insolation forcing and the associated reduction and southward shift over the region of the boreal monsoon flow (Bassinot et al., 2011). Short term variability is also present. This variability is internal to the coupled system and is thus not synchronous between the simulations. However, the major events are synchronous between the latitudes, and major transitions seem also to be synchronous across the simulations, suggesting a response to a common forcing or to the same feedback from the ocean

circulation or vegetation. In particular, all simulations exhibit a rapid precipitation decrease around 5000 cal yr BP that occurs in several steps. The two accelerated simulation also exhibit periods with enhanced variability after 2000 cal yr BP. Even though both simulations do not change at the exact same time, we can conclude that this stochastic variability seems to be related to favorable conditions in the mean state. Further analyses to fully understand this is however outside the scope of the manuscript.

3. Timing of environmental changes and linkage with the timing of the southward shift of the summer monsoon rainbelt (Fig. 6)

The analyses of the evolution of vegetation at the two sites and the ensemble of IPSL-CM5A simulations allow us to infer the long term changes and variability of the ITCZ rainbelt over the Arabian Sea and Arabian Peninsula. We have calculated two indices illustrating the local and regional evolution of the environment. The *Avicennia/Rhizophora* ratio compares a salt-adapted (*Avicennia*) to a fresh-water-adapted (*Rhizophora*) species (Spalding et al., 1997). This ratio aims at representing the fluctuations between freshwater and saline conditions locally, at each mangrove site. In addition, the *Artemisia/Rhizophora* ratio compares one of the most arid components of the regional environment typically *Artemisia* today mainly found north of the Arabian Peninsula in areas under Mediterranean climate conditions (El-Moslimany, 1990) to one of the most humid components of the environment characteristic of tropical climate conditions (*Rhizophora)*. These ratios highlight the occurrence of two opposing phases during the mid to late Holocene. We discuss in the following the linkages between these phases and the location of boreal summer monsoon rainbelt (i.e., the limit between the zones of influence of winter and summer rains). For this, we compare our data to the oxygen isotope records of speleothems at Qunf and Hoti in southern Oman (Neff et

al., 2001; Fleitmann et al., 2003; 2007) and the dated records of past lakes and wetlands in the Arabian Peninsula (Lézine et al., 2014, Fersi et al., 2016) (Supplementary Table 2) (Fig. 5) and to the climate simulations.

3.1 From 7500 to 2700 cal yr BP (Filim) and from 6358 to 4500 cal yr BP (Kwar-al-Jaramah): a summer monsoon-dominated climate regime

At both sites, the pollen record is characterized by the presence of *Rhizophora* (Fig. 3). Percentages of this taxon reach 43 to 52% at Filim during a time interval from 6800 to 6700 cal yr BP, that clearly indicate the presence of a developed freshwater mangrove forest at the core site. Then percentages decrease in two successive steps at ca. 6000 then 4500 cal yr BP. After 2700 cal yr BP, *Rhizophora* pollen grains become scarce and their percentages never exceed 2%. At Kwar-al-Jaramah, *Rhizophora* peaks at 13.5% only (4960-5100 cal BP), showing a less developed forest formation compared to the southernmost site. These percentages decrease rapidly, and *Rhizophora* almost completely disappears from the pollen diagram after 4500 cal yr BP. The presence of *Rhizophora* within the mangrove forests of Oman clearly points to the tropical influence and associated enhanced summer rainfall. We suggest that SW summer monsoon winds were responsible for the transport of tropical pollen grains from the Dhofar region, not only at Filim but also at Kwar-al-Jaramah.

During the mid-Holocene, the tropical influence covered a wide range of latitudes as shown by the isotope records (Neff et al., 2001; Fleitmann et al., 2003; 2007) and various lacustrine deposits over southern Arabia (Lézine et al., 2014 and references therein; Fersi et al., 2016) (Supplementary Table 2). This is also illustrated by the presence of *Rhizophora* populations reported at al-Balid at 17°N (Zarins, 2007), Suwayh at 22°N (Lézine et al., 2002), and tell Abraq at 25°N (Tengberg, 2005), as well as by multiple geomorphological observations and

308 archaeological findings along the Ja'alan coast in Oman (Giraud, 2009; Berger et al., 2013)
309 suggesting widespread expansion of mangroves all along the Arabian coasts at that time.
310 Wind roses computed over the large area that encompass all the sites show the June-July-
311 August (JJA) and the evolution of simulated precipitation are in agreement with this
312 assumption (Fig. 4 - 6). A rapid humid-arid transition around 5000 cal yr BP is depicted both
313 in pollen records and in all simulations. It indicates that the insolation forcing is the major
314 driver of this rapid decrease, suggesting that around that time, the meridional insolation
315 gradient was not sufficient to maintain the associated pressure gradients driving the SW
316 monsoon flow over the region. The rapid shifts indicate that the northern limit of the
317 rainbelt did not rich the pollen sites and the abruptness of the shift is the signature of a
318 threshold in amount of moisture necessary to maintain the vegetation there. This explains
319 the connection between the disappearance of *Rhizophora* and the southward shift of the
320 rainbelt.
321
322 **3.2 At 2700 cal yr BP, the reversal of main wind trajectories**
323 From 2700 cal yr BP onward, the disappearance of *Rhizophora* was mirrored by the
324 development of *Prosopis cineraria*. This marks the reversal of the main regional climatic
325 influences with the decreased importance of the SW Indian summer monsoon and the
326 increased importance of Mediterranean wind fluxes of opposite direction. *Prosopis* occurred
327 continuously at Ras al-Khaimah, Eastern Arabia (25° 42' 57''N) from 8500 cal yr BP to the
328 present (Parker et al., 2004) and at Kwar-al-Jaramah from 6358 cal yr BP onwards (this
329 study). It was absent at Suwayh (22°05N) before 4000 cal yr BP (Lézine et al., 2002) and at
330 Filim before 2700 cal yr BP (this study). As a consequence, we can suggest that the limit
331 between the summer and the winter rains was situated between Kwar-al-Jaramah and

Suwayh ca 22°30 N during the mid-Holocene. At 2700 cal yr BP, it was displaced southward and situated at its present-day position between 18 and 19°N (Ghazanfar and Fischer, 1998). Climate simulations are consistent with this scenario. In addition, the two transient simulations suggest declining SW monsoon flux together with a period of enhanced variability after 2000 cal yr BP. Such enhanced variability and the associated increase of rainy events could have contributed to feed lakes and wetlands in the Arabian Peninsula (Fig. 6). The events are not synchronous between the simulations, suggesting that the large scale circulation is suitable for the development of periods with higher variability, but that this variability is not a direct response to an external forcing and appears thus at different times in the two simulations.

4. Concluding remarks

Our study, based on transient climate simulations compared to high resolution and well distributed paleo-data provide for the first time a detailed chronology of the retreat of the rain belt associated to the southward shift of the ITCZ at the end of the Holocene in Eastern Arabia. This approach paves the way to a thorough understanding of rainfall variations and their impact on terrestrial ecosystems in arid areas.

Figure 6 shows that the timing and structure of the arid-humid transition strongly varied with latitude, such that north of 22°30 N, the humid-arid transition was abrupt at all latitudes. The southward shift of the rainbelt took place at 6026 cal yr BP at Hoti (Fig. 6F), then at 4500 cal yr BP at Kwar-al-Jaramah (Fig. 5D). In contrast, the increase in regional dryness was gradual south of 20°30 N as shown by the Qunf isotope record (Fig. 6B) and the *Artemisia/Rhizophora* ratio at Filim (Fig. 6C) and reached its maximum at 2700 cal yr BP. Both data and climate simulations agree that two major successive thresholds occurred at

ca. 4500-5000 cal yr BP and 2700 cal yr BP and punctuated the southward retreat of the ITCZ and associated rainbelt at the end of the Holocene Humid Period in Southern Arabia.

- All simulations (Fig. 6F) exhibit a sharp decrease in precipitation around 4500-5000 cal yr BP. This first threshold coincides with the dramatic lowering of the water bodies in Southern Arabia (Fig. 5A) and the onset of arid conditions throughout the tropics in response to insolation forcing. A comparison of environmental conditions between Filim and Kwar-al-Jaramah help to more precisely locate the position of the ITCZ at ca. 22°30 N.
- At the time of the second threshold identified at 2700 cal yr BP, aridity was pervasive all over Southern Arabia. This second threshold corresponds not only to the disappearance of *Rhizophora* from the mangroves of Filim and the widespread expansion of *Prosopis cineraria* along the coasts of Oman, but also to the interruption of speleothem growth (Fleitmann et al., 2003; 2007) and river activity (Hoorn and Cremaschi, 2004) in Southern Oman. The beginning of very dry conditions and the prevalence of wind fluxes of NE origin at that time were already observed at Lake Yoa, Northern Chad (Lézine et al., 2010). Climate instability characterized by increased rainy events may have however contributed to the slight elevation of the lake levels observed towards the end of the period in Southern Arabia and particularly during the last millennium.

Acknowledgements

This research was funded by the national research funding agency in France (ANR) through three distinct projects: “SOPHOCLE” (ANR-05-BLAN-0352), “SAHELP” (ANR-06-VULN-0015) and “ELPASO” (ANR-10-BLAN-0608). Thanks are due to late Serge Cleuziou (CNRS) and late

Jean-François Saliège (UPMC) for their constant friendship and their exceptional scientific expertise as well as to Jean-Jacques Tiercelin (CNRS), Jean-Paul Breton (BRGM) and Jean-Pierre Cazet (CNRS) for assistance with core collection and processing. We thank the Ministry of Heritage and Culture and the Ministry of Commerce and Industry, Muscat, for authorizations and support. AMS dating was provided by UMS-ARTEMIS (Saclay, France) AMS Facilities. A.-M.L. is supported by CNRS (France) and P.B. and O.M. by CEA (France). S.I. stay in France was funded by the French project ANR-06-VULN-0015. Paleohydrological data used Fig 6A (Supplementary Table 2) are available from the NOAA Paleoclimatology Data Center. Pollen data from Filim and Kwar-al-Jaramah are available from the first author.

References

Bayon, G., Dennielou, B., Etoubleau, J., Ponzevera, E., Toucanne, S., Bermell, S. 2012. Intensifying weathering and land use in Iron Age Central Africa. Science 335, 1219-1222.

Bassinot, F.C., Marzin, C., Braconnot, P., Marti, O., Mathien-Blard, E., Lombard, F., Bopp, L. 2011. Holocene evolution of summer winds and marine productivity in the tropical Indian Ocean in response to insolation forcing: data-model comparison. Clim. Past 7, 815-829.

Berger, A. 1978. Long-term variations of caloric solar radiation resulting from the Earth's orbital elements. Quatern. Res. 9, 139-167.

Berger, J.-F., Charpentier, V., Crassard, R., Martin, C., Davtian, G., Lopez-Saez, J.A. 2013. The dynamics of mangrove ecosystems, changes in sea level and the strategies of Neolithic settlements along the coast of Oman (6000-3000 cal. BC). J. Archaeol. Sci. 40, 3087-3104.

Bird, M.I., Austin, W.E.N., Wurster, C.M., Fifield, L.K., Mojtahid, M., Sargeant, C., 2010. Punctuated eustatic sea-level rise in the early mid-Holocene. Geology 38, 803–806.

Bonnefille, R., Riollet, G. 1980. Pollens des savanes d'Afrique orientale, CNRS, Paris, 140 p.

Braconnot, P., Harrison, S.P., Kageyama, M., Bartlein, P.J., Masson-Delmotte, V., Abe-Ouchi, A., Otto-Bliesner, B., Zhao, Y., 2012. Evaluation of climate models using palaeoclimatic data. Nature Clim. Change, 2,417-424.

Claussen, M., Brovkin, V., Ganopolski, A., Kubatzki, C., Petoukhov, V. 2003. Climate Change in Northern Africa: The Past is Not the Future. Clim. Change 57, 99.

Claussen, M., Gayler, V. 1997. The greening of the Sahara during the mid-Holocene: results of an interactive atmosphere-biome model. Global Ecol. Biogeogr. 6, 369–377.

deMenocal, P., Ortiz, J., Guilderson, T., Adkins, J., Sarnthein, M., Baker, L., Yarusinsky, M. 2000 Abrupt onset and termination of the African Humid Period: rapid climate responses to gradual insolation forcing. Quatern. Sci. Rev. 19, 347–361.

Dufresne, J. L., Foujols, M. A., Denvil, S., Caubel, A., Marti, O., Aumont, O., Balkanski, Y., Bekki, S., Bellenger, H., Benshila, R., Bony, S., Bopp, L., Braconnot, P., Brockmann, P., Cadule, P., Cheruy, F., Codron, F., Cozic, A., Cugnet, D., de Noblet, N., Duvel, J. P., Ethe, C., Fairhead, L., Fichefet, T., Flavoni, S., Friedlingstein, P., Grandpeix, J. Y., Guez, L., Guilyardi, E., Hauglustaine, D., Hourdin, F., Idelkadi, A., Ghattas, J., Joussaume, S., Kageyama, M., Krinner, G., Labetoulle, S., Lahellec, A., Lefebvre, M. P., Lefevre, F., Levy, C., Li, Z. X., Lloyd, J., Lott, F., Madec, G., Mancip, M., Marchand, M., Masson, S., Meurdesoif, Y., Mignot, J., Musat, I., Parouty, S., Polcher, J., Rio, C., Schulz, M., Swingedouw, D., Szopa, S., Talandier, C., Terray, P., Viovy, N., and Vuichard, N. 2013. Climate change projections using the IPSL-CM5 Earth System Model: from CMIP3 to CMIP5. Clim. Dyn. 40, 2123-2165.

El-Baz, F. 2002. Wadis of Oman, satellite images. Atlans. Sultanate of Oman, Office of the Advisor to His Majesty The Sultan for Cultural Affairs. 218 p.

El-Ghazali, G. 1991. Pollen flora of Qatar. Scientific and applied research Center, University of Qatar, 429 p.

Faegri, K., Iversen, J., 1975. Textbook of Pollen Analysis. Blackwell, Oxford.

Farooki, A., Gaur, A.S., Prasad, V. 2013. Climate, vegetation and ecology during Harappan period: excavations at Kanjetar and Kaj, mid-Saurashtra coast, Gujurat. J. Archaeol. Sci. 40, 2631-2647.

Fichefet, T., Maqueda, M.A.M. 1997. Sensitivity of a global sea ice model to the treatment of ice thermodynamics and dynamics. J. Geophys. Res., Oceans 102, C6, 12609 -12646.

Fleitmann, D., Burns, S.J., Mangini, A., Mudelsee, M., Kramers, J., Villa, I., Neff, U., Al-Subbary, A.A., Buettner, A., Hippler, D., Matter, A. 2007. Holocene ITCZ and Indian monsoon dynamics recorded in stalagmites from Oman and Yemen (Socotra). Quatern. Sci. Rev. 26, 170-188.

Fleitmann, D., Burns, S.J., Mudelsee, M., Neff, U., Kramers, J., Mangini, A., Matter, A. 2003. Holocene Forcing of the Indian Monsoon Recorded in a Stalagmite from Southern Oman. Science 300, 1737-1739.

Gasse, F. 2000. Hydrological changes in the African tropics since the Last Glacial maximum. Quatern. Sci. Rev. 19, 189-211.

Giraud, J. 2009. The evolution of settlement patterns in the eastern Oman from the Neolithic to the Early Bronze Age (6000-2000 BC). C. R. Geoscience 341, 739-749.

Ghazanfar, S.A., Fisher, M., 1998. Vegetation of the Arabian Peninsula. Geobot. 25, 1-362.

450 Harrison, S. P., Bartlein, P. J., Izumi, K., Li, G., Annan, J., Hargreaves, J., Braconnot, P.,
451 Kageyama, M. 2015. Evaluation of CMIP5 palaeo-simulations to improve climate
452 projections. Nature Clim. Change 5, 735-743.
453 Hély, C., Lézine, A.-M. and APD contributors. 2014. Holocene changes in African vegetation:
454 tradeoff between climate and water availability. Clim. Past 10, 681-686.
455 Hoorn, C., Cremaschi, M. 2004. Late Holocene palaeoenvironmental history of Khawr Rawri
456 and Kwar-al-Balid (Dhofar, Sultanate of Oman). Palaeogeogr., Palaeoclim., Palaeoecol.
457 213, 1-36.
458 Hourdin, F., Musat, I., Bony, S., Braconnot, P., Codron, F., Dufresne, J.L., Fairhead L., Filiberti
459 M.A., Friedlingstein P., Grandpeix J.Y., Krinner G., LeVan P., Li Z.X., Lott F. 2006. The
460 LMDZ4 general circulation model: climate performance and sensitivity to parametrized
461 physics with emphasis on tropical convection. Clim. Dyn. 27, 787–813.
462 Jousse, H., Escarguel, G. 2006. The use of Holocene bovid fossils to infer palaeoenvironment
463 in Africa. Quatern. Sci. Rev. 25, 763-783.
464 Kageyama, M., Braconnot, P., Bopp, L., Caubel, A., Foujols, M.-A., Guilyardi, E., Khodri, M.,
465 Lloyd, J., Lombard, F., Mariotti, V., Marti, O. 2013. Mid-Holocene and Last Glacial
466 Maximum climate simulations with the IPSL model—part I: comparing IPSL_CM5A to
467 IPSL_CM4. Clim. Dyn. 40, 2447-68.
468 Krinner, G., Viovy, N., de Noblet-Ducoudré, N., Ogée, J., Polcher, J., Friedlingstein, P., Ciais,
469 P., Sitch, S., Prentice, I.C. 2005. A dynamic global vegetation model for studies of the
470 coupled atmosphere–biosphere system. Global Biogeochem. Cycles.
471 doi:10.1029/2003GB002199
472 Kuper, R., Kröpelin, S. 2006. Climate-controlled Holocene occupation in the Sahara: motor of
473 Africa's evolution. Science 313, 803–807.

474 Kutzbach, J.E., Street-Perrott, F.A. 1985. Milankovitch forcing of fluctuations in the level of
475 tropical lakes from 18 to 0 k yr BP. Nature 317, 130–134.
476 Lambeck, K., 1996. Shoreline reconstructions for the Persian Gulf since the last glacial
477 maximum. Earth Planet. Sci. Let. 142, 43-57.
478 Lézine, A.-M. 2009. Timing of vegetation changes at the end of the Holocene Humid Period
479 in desert areas at the northern edge of the Atlantic and Indian monsoon systems. C.R.
480 Geoscience 341, 750-759.
481 Lézine, A.-M., Bassinot, F., Peterschmitt, J.-Y. 2014. Orbitally-induced changes of the Atlantic
482 and Indian monsoons over the past 20,000 years: new insights based on the comparison
483 of continental and marine records. Bull. Soc. Géol. France 185, 3-12.
484 Lézine, A.-M., Hély, C., Grenier, C., Braconnot, P., Krinner, G. 2011. Sahara and Sahel
485 vulnerability to climate changes, lessons from Holocene hydrological data. Quatern. Sci.
486 Rev. 30, 3001-3012.
487 Lézine, A.-M., Robert, C., Cleuziou, S., Inizan M.-L., Braemer, F., Saliège, J.-F., Sylvestre, F.,
488 Tiercelin, J.-J., Crassard R., Méry, S., Charpentier, V., Steimer-Herbet, T. 2010. Climate
489 Evolution and Human Occupation in the Southern Arabian lowlands during the last
490 deglaciation and the Holocene. Glob. Planet. Change 72, 4, 412-428
491 Lézine, A.-M., Saliège, J.-F., Mathieu, R., Tagliatela, T.L., Mery, S., Charpentier, V., CLeuziou,
492 S. 2002. Mangroves of Oman during the late Holocene: climatic implications and impact
493 on human settlements. Veget. Hist. Archaeobot. 11, 221-232.
494 Liu, Z., Wang, Y., Gallimore, R., Gasse, F., Johnson, T., deMenocal, P., Adkins, J., Notaro, M.,
495 Prentice, I.C., Kutzbach, J., Jacob, R., Behling, P., Wang, L., Ong, E. 2007. Simulating the
496 transient evolution and abrupt change of Northern Africa atmosphere–ocean–terrestrial
497 ecosystem in the Holocene. Quatern. Sci. Rev. 26, 1818–1837.

498 Lorenz, S. J., Lohmann, G. 2004. Acceleration technique for Milankovitch type forcing in a
499 coupled atmosphere-ocean circulation model: method and application for the Holocene.
500 Clim. Dyn. 23, 727-743.
501 Maley, J. 1970. Contribution à l'étude du bassin tchadien : atlas des pollens du Tchad. Bull.
502 du J. Bot. Nat. Belgique 40, 29-48.
503 Manning, K., Timpson, A. 2014. The demographic response to Holocene climate change in
504 the Sahara. Quatern. Sci. Rev. 101, 28-35.
505 Marzin, C., Braconnot, P. 2009. Variations of Indian and African monsoons induced by
506 insolation changes at 6 and 9.5 kyr BP. Clim. Dyn. 33, 215-231.
507 Miller, A.G., Morris, M. 1988. Plants of Dhofar. The Office of the Adviser for Conservation of
508 the Environment, Diwan of Royal Court Sultanate of Oman, 361 p.
509 Morrill, C., Overpeck, J.T., Cole, J.E. 2003. A synthesis of abrupt changes in the Asian summer
510 monsoon since the last deglaciation. The Holocene 13, 465-476.
511 Neff, U., S.J. Burns, A. Mangini, M. Mudelsee, D. Fleitmann, and A. Matter. 2001. Strong
512 coherence between solar variability and the monsoon in Oman between 9 and 6 kyr
513 ago. Nature 411, 290-293.
514 Overpeck, J., Anderson, D., Trumbore, S., Prell, W. 1996. The southwest Indian Monsoon
515 over the last 18 000 years. Clim. Dyn. 12, 213–225.
516 Reimer, P.J., Baillie, M.G., Bard, E., Bayliss, A., Beck, J.W., Blackwell, P.G., Bronk, R.C., Buck,
517 C.E., Burr, G.S., Edwards, R.L., Friedrich, M. 2009. IntCal09 and Marine09 radiocarbon
518 age calibration curves, 0-50,000 years cal BP. Radiocarbon 51, 1111–1150.
519 Saint-Lu, M., Braconnot, P., Leloup, J., Lengaigne, M., Marti, O. 2015. Changes in the
520 ENSO/SPCZ relationship from past to future climates. Earth Planet. Sci. Let. 412, 18-24.

521 Saliège, J.-F., Lézine, A.-M., Cleuziou, S. 2005. Estimation de l'effet réservoir 14C marine en
522 mer d'Arabie. Paléorient 31,1, 64-69.
523 Spalding, M., Blasco, F., Field, C. 1997. The world mangrove atlas. Okinawa, Japan,
524 International Society for Mangrove Ecosystems, 178 p.
525 Tengberg, M. 2005. Les forêts de la mer. Exploitation et évolution des mangroves en Arabie
526 orientale du Néolithique à l'époque islamique. Paléorient 31, 39-45.
527 Valcke, S. 2006. OASIS3 user guide (prism_2-5). PRISM Support Initiative Rep. 3,64p.
528 Zarins, J. 2007. Aspects of recent archaeological work at al-Balid (Zafar), Sultanate of Oman.
529 Proceed. Semin. Arab. Stud. 37, 309-324.

Figure Captions

Figure 1: Modern surface winds at 925 hP for summer and winter months (NCEP-DOE AMIP-II Reanalysis) and location of the sites in the text: Kwar-al-Jaramah (KAJ) and Filim : pollen, this study; Qunf and Hoti: speleothems, Neff et al., 2001; Fleitmann et al., 2003; 2007. Aerial views from El-Baz (2002).

Figure 2: *Avicennia marina* mangroves at Filim (A, B) and Kwar-al-Jaramah (C, D)

Figure 3: Simplified pollen diagrams at Filim and Kwar-al-Jaramah showing the percentages of the main pollen taxa over time. In grey x20 magnification.

Figure 4: Surface winds as simulated by the IPSL-CM5A climate model: Surface winds (m/s) for (A) summer (JA) and (B) winter (JF) months for three periods PI, 4ka, and 6ka (B) and wind roses (wind strength in m/s and frequency in %) for (C) summer and (D) winter for the same three periods: 6k (green), 4ka (blue), and PI (black).

Figure 5: Long-term evolution of June-July-August precipitation (mm/day) between 14-18, 18-20 and 20-24°N; A : transient IPSL simulation from 6000 to 3900 cal yr BP and B : two IPSL transient simulations from 6000 cal yr BP to zero for which changes in earth orbital parameters have been accelerated by a factor 10 (see details in the text). These two simulations have different initial states. The curves have been smoothed by an equivalent hundred years in A (100 yrs) and B (10 yrs) (bold lines).

Figure 6: The end of the Holocene Humid Period in Southern Arabia: multiproxy records and climate simulations. A: dated records of lakes, wetlands, and rivers at 1000 year intervals (Lézine et al., 2014. See paleohydrological database and reference therein at NOAA), B:Qunf speleothem isotope record (Fleitmann et al., 2003; 2007), C and D: local (*Avicennia/Rhizophora*) and regional (*Artemisia/Rhizophora*) indexes of aridity at Filim (C) and Kwar-al-Jaramah (D), E: Hoti speleothem isotope record (Neff et al., 2001), F: hundred

554 year smoothed transient IPSL simulations for the time interval between 6000 cal yr BP and
555 present day (cf Fig. 4).

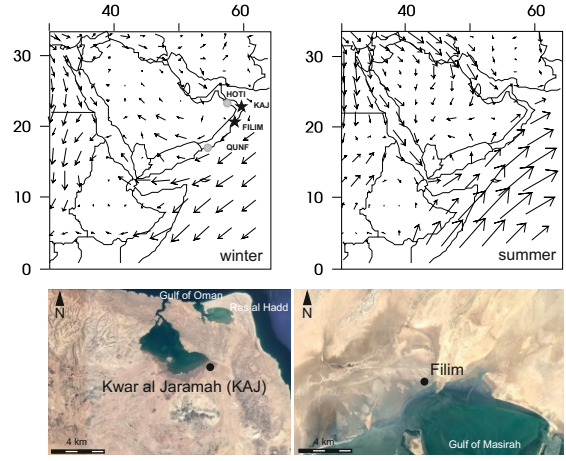
40
60
30
20
10
0
HOTI
KAJ
FILIM
QUNF
winter
summer

N
Gulf of Oman
Ras al Hadd
Kwar al Jaramah (KAJ)
4 km

N
Filim
4 km
Gulf of Masirah


A


B


C


D

FILIM (OMAN) Main taxa

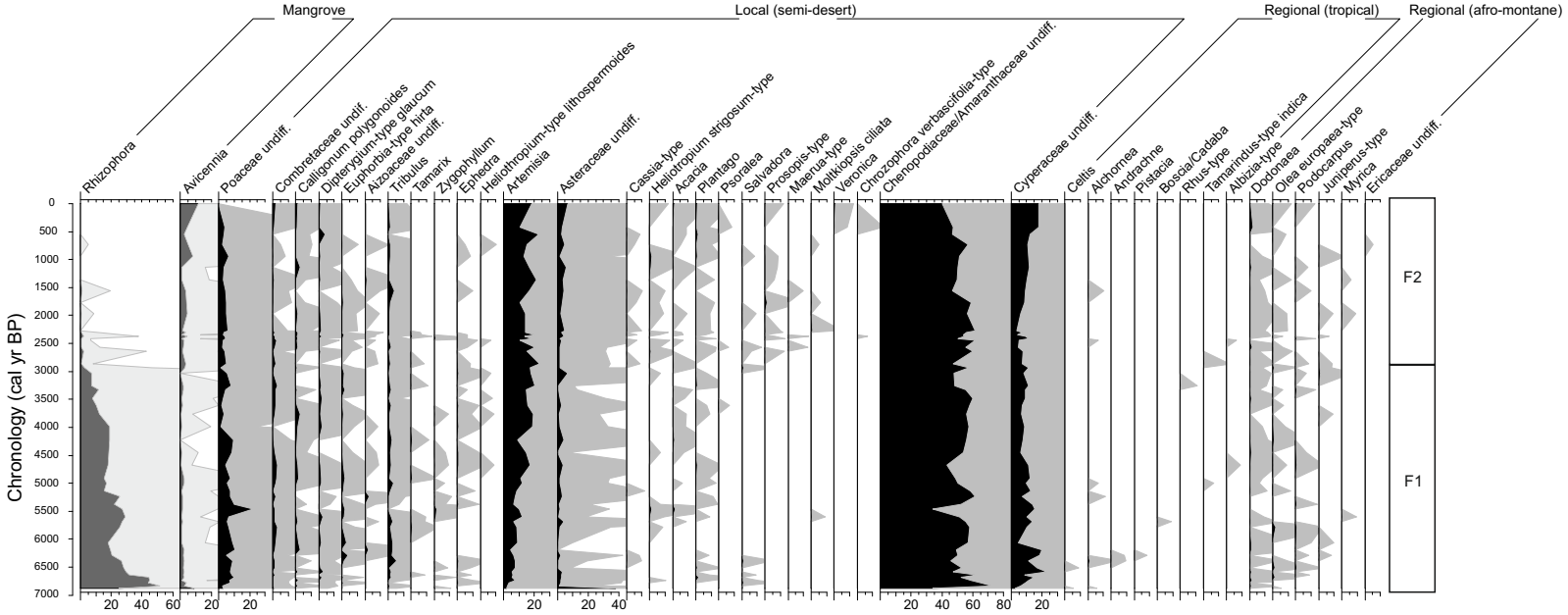

KWAR AL JARAMAH (OMAN) Main taxa

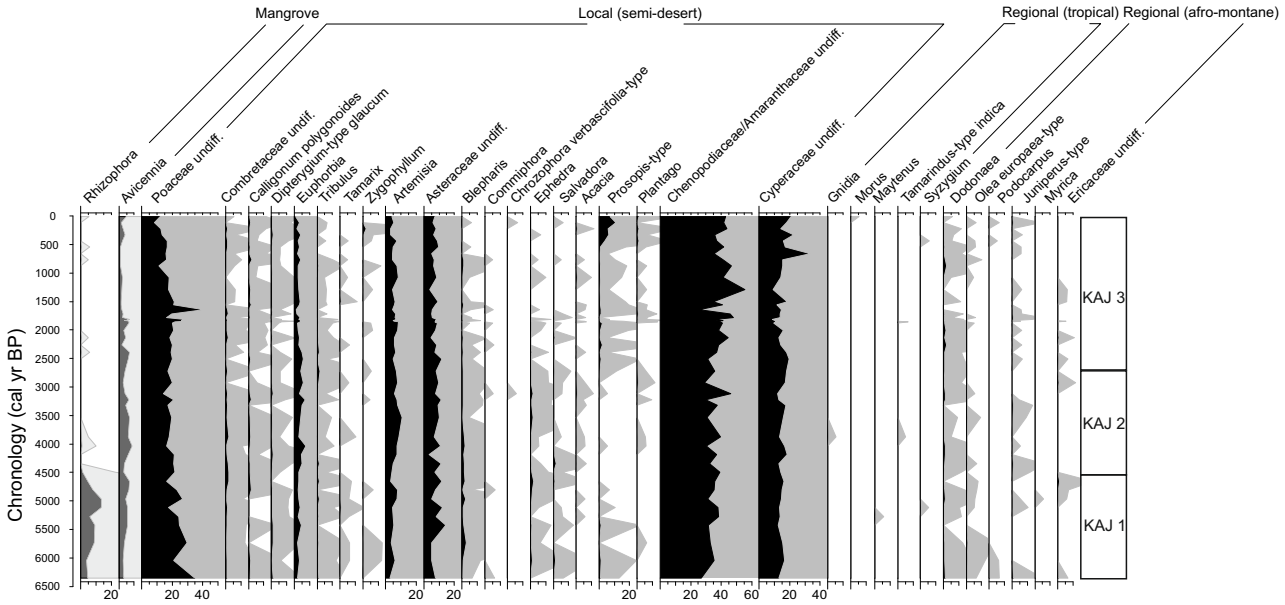

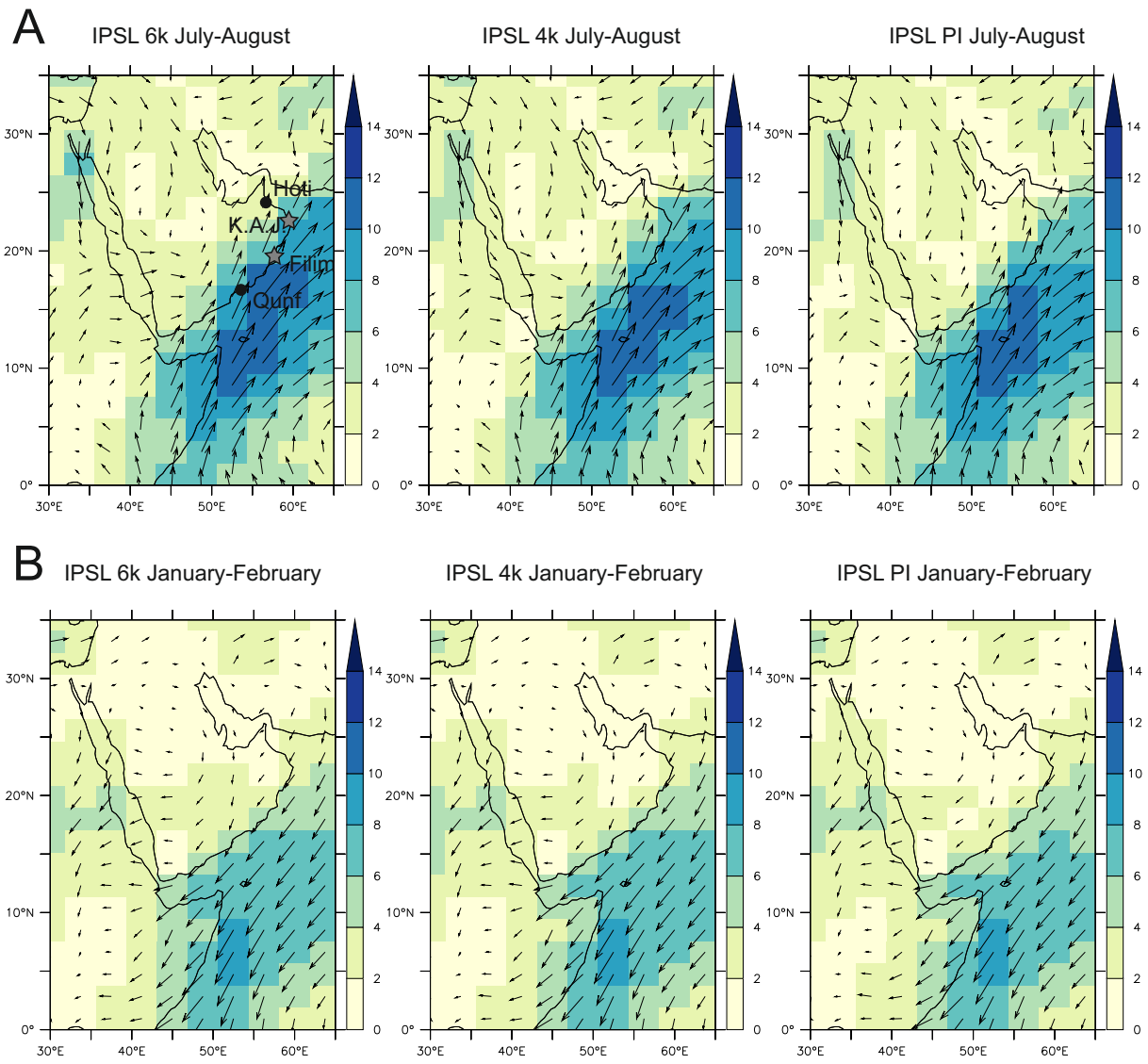
A
IPSL 6k July-August
IPSL 4k July-August
IPSL PI July-August
Hoti
K.A.J.
Filim
Qunf
30°N
20°N
10°N
0°
30°E
40°E
50°E
60°E
0
2
4
6
8
10
12
14

B
IPSL 6k January-February
IPSL 4k January-February
IPSL PI January-February
30°N
20°N
10°N
0°
30°E
40°E
50°E
60°E
0
2
4
6
8
10
12
14

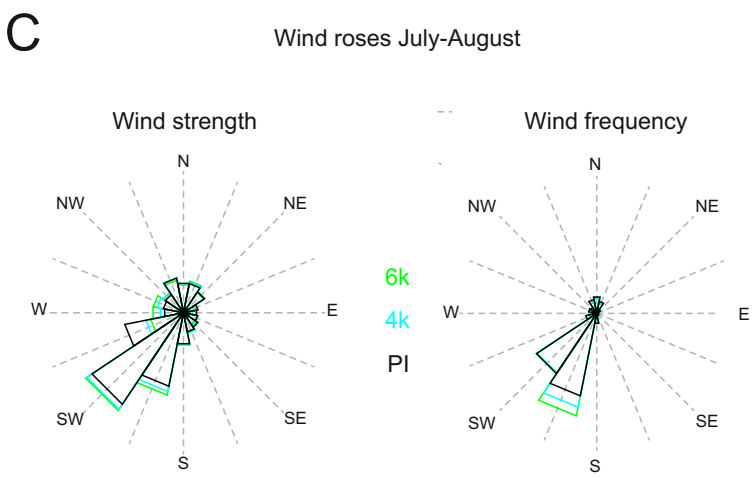
C
Wind roses July-August
Wind strength
Wind frequency
6k
4k
PI
N
NE
E
SE
S
SW
W
NW

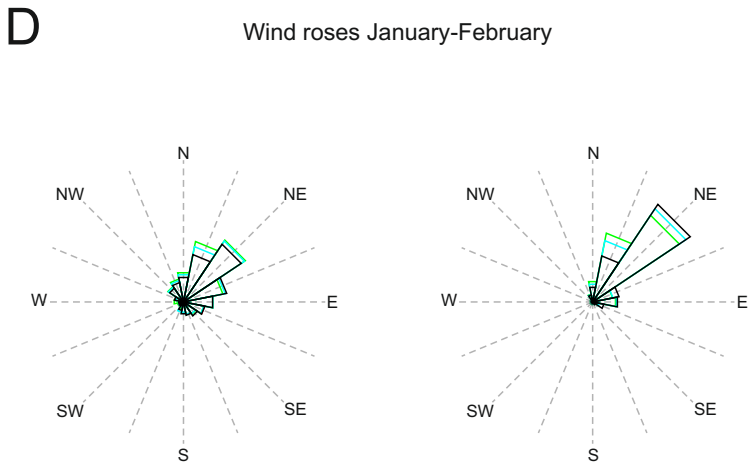
D
Wind roses January-February
N
NE
E
SE
S
SW
W
NW

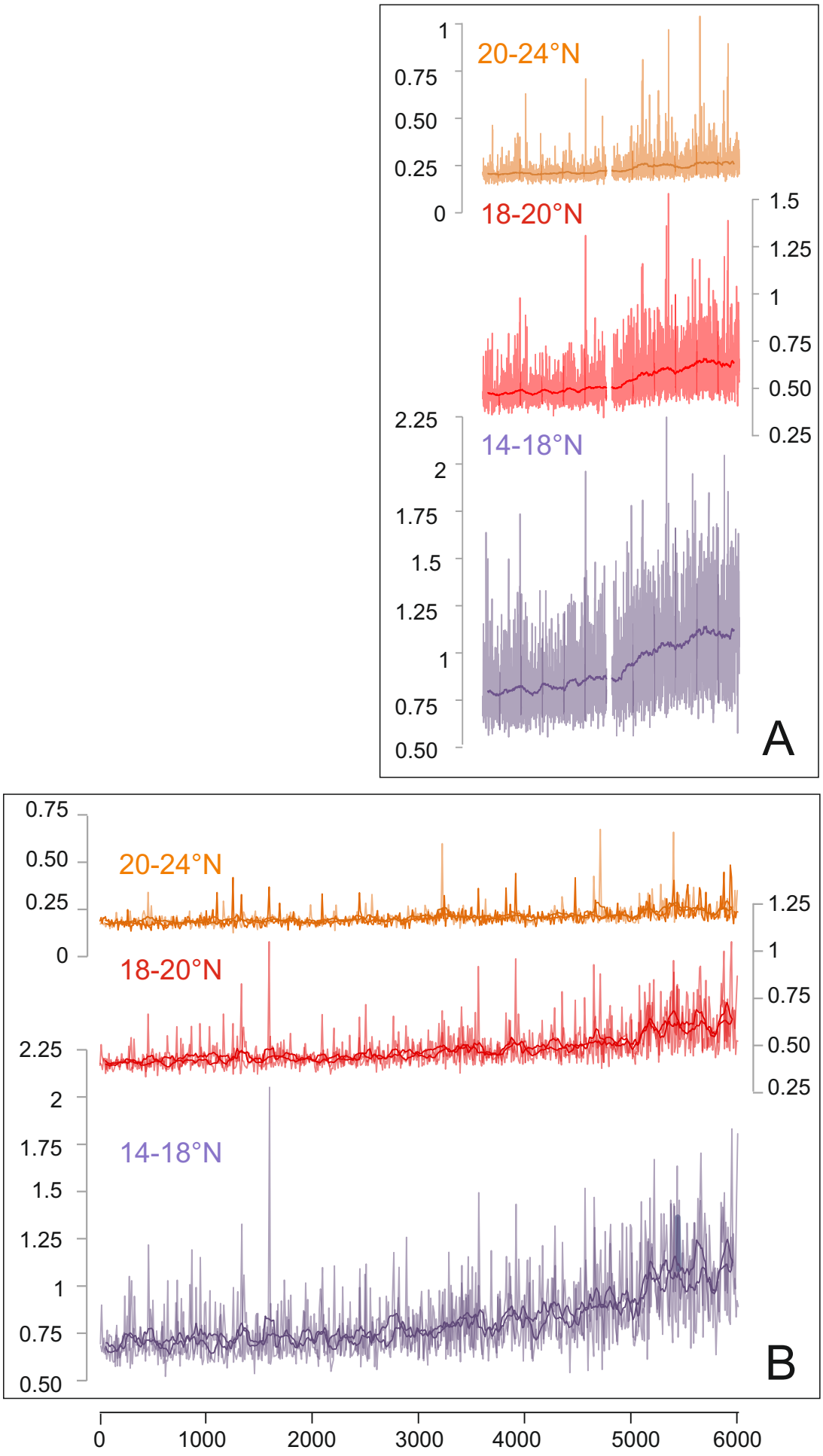
20-24°N
18-20°N
14-18°N
A
B
0.75
0.50
0.25
0
1
1.25
1.5
1.75
2
2.25
0
1000
2000
3000
4000
5000
6000
Chronology (cal yr BP)

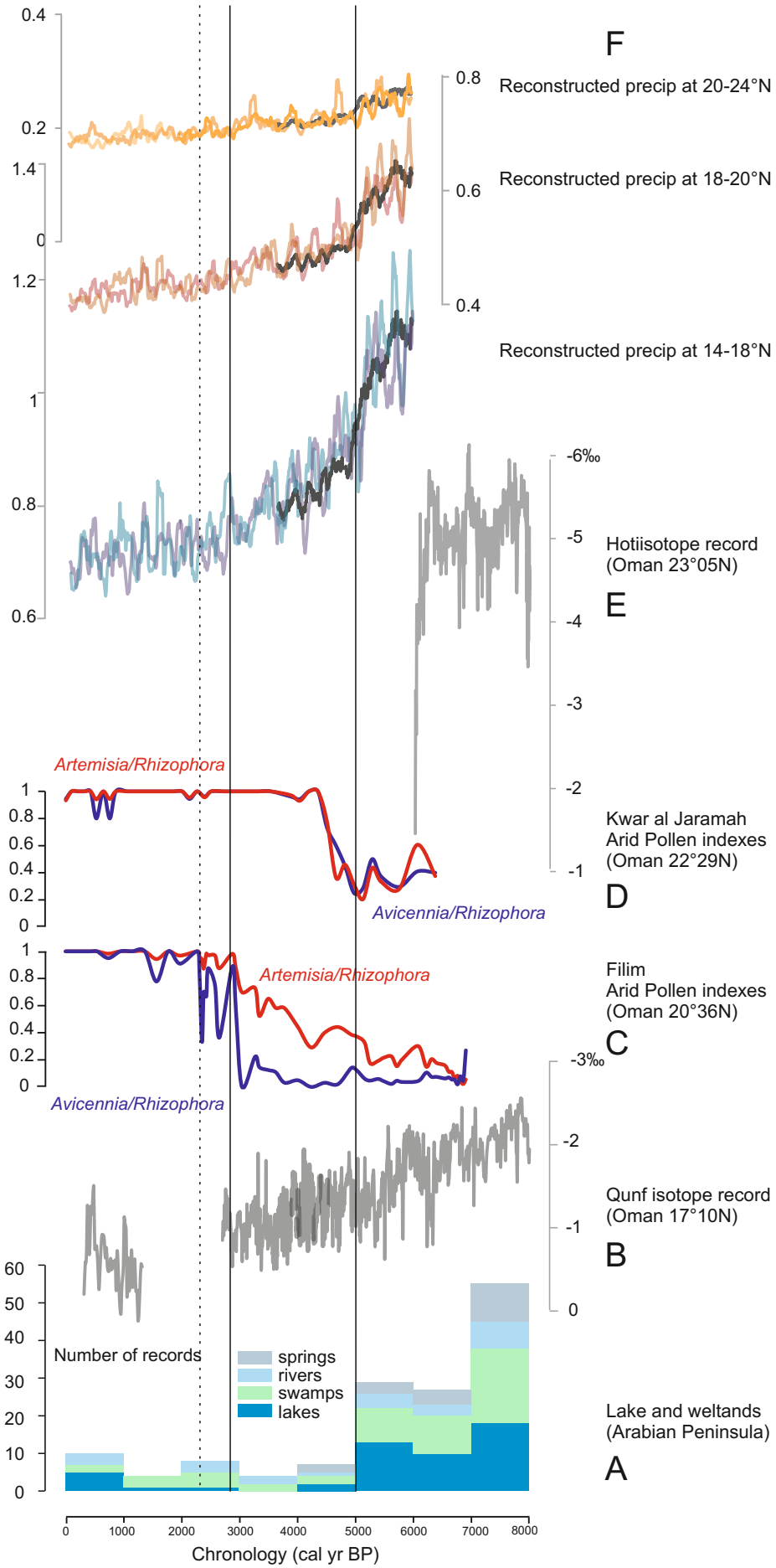
F
Reconstructed precip at 20-24°N
Reconstructed precip at 18-20°N
Reconstructed precip at 14-18°N
Hotiisotope record
(Oman 23°05N)
E
Artemisia/Rhizophora
Avicennia/Rhizophora
Kwar al Jaramah
Arid Pollen indexes
(Oman 22°29N)
D
Artemisia/Rhizophora
Avicennia/Rhizophora
Filim
Arid Pollen indexes
(Oman 20°36N)
C
Qunf isotope record
(Oman 17°10N)
B
Number of records
springs
rivers
swamps
lakes
Lake and weltands
(Arabian Peninsula)
A
Chronology (cal yr BP)

Depth (cm)	14C	material	Lab number	1 sigma calendar year (ΔR= 210±15)
55-56	1060±30	shells	SacA 7200	456-505
105-106	1345±30	shells	SacA 7201	654-712
149-150	1790±50	shells	SacA 7202	1074-1207
205-206	2810±45	shells	SacA 7203	2207-2334
215-216	3810±30	shells	SacA 7205	3445-3544
305-306	4025±30	shells	SacA 7208	3709-3818
365-366	6305±30	shells	SacA 7209	6465-6574
404-406	6475±30	shells	SacA 7210	6665-6759

Table 1a: Filim chronological control. AMS on marine shells (Saclay Artemis AMS Facilities). Calibrated ages from Reimer et al. (2009) applying the local Δ R calculated by Saliège et al. (2005).

Depth (cm)	14C	material	Lab number	1 sigma calendar year (ΔR= 210±15)
70-71	1445±30	shells	SacA 7217	722-820
149-150	2245±30	shells	SacA 7219	1548-1653
205-206	2415±30	shells	SacA 7220	1757-1858
249-250	2480±30	shells	SacA 7221	1829-1922
299-300	3270±30	shells	SacA 7222	2770-2262
345-346	3760±40	shells	SacA 7223	3372-3484
399-400	5010±35	shells	SacA 7224	5011-5194

Table 1b: Kwar-al-Jaramah chronological control on marine shells (Saclay Artemis AMS Facilities). Calibrated ages from Reimer et al. (2009) applying the local Δ R calculated by Saliège et al. (2005).

Period	Excentricity	Obliquity	Perihelion – 180.
PI	0.0167	23.446	102.04
4ka	0.0181	23.929	34.26
6ka	0.0187	24.105	0.87

Table 2: Orbital parameters prescribed in the different time slice experiments.